Electronic Supplementary Material (ESI) for Journal of Materials Chemistry C.
This journal is © The Royal Society of Chemistry 2023

LTP-LTD Transformation of Unipolar Pulse Voltage-Driven Zinc Oxide Memristors Via TiO_2 Thin Layer Incorporation

Yucheng Wang[a1], Jiawei Zheng[a1], Yueyang Shang[1], Dingyun Guo[1], Hexin Wang[1], Zeyang An[1], XiaoChuan Chen[1], Ruixi Huang[1], JunYu Jiang[1], Kai Sun[2], Shaoxi Wang[*1]

[1]School of Microelectronics, Northwestern Polytechnical University, Xi'an, 710072, China.

[2]School of Microelectronics, Xidian University, Xi'an, 710072, China

*Corresponding author. E-mail: shxwang@nwpu.edu.cn

[a]These authors contributed equally to this work.

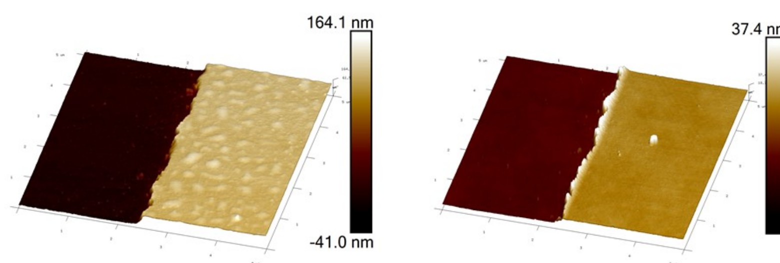

Figure S1 AFM image of ZnO film and TiO_2 thickness.

According to the AFM test results in Figure S1, the thickness of the ZnO and TiO_2 functional layers are 101.5 nm and 11.4 nm, respectively.

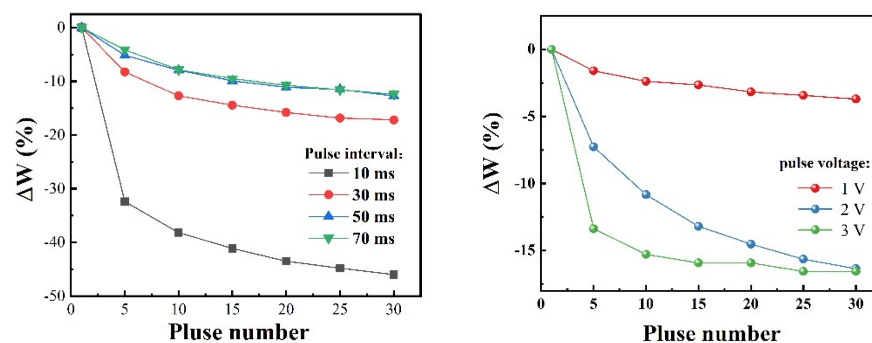

Figure S2 The influence of different pulse interval and pulse amplitude on ΔW is studied.

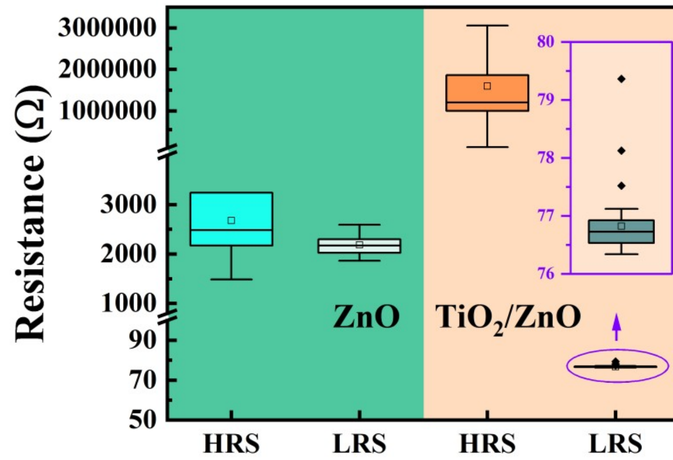

Figure S3 HRS and LRS of single-layer devices and double-layer devices.

Figure S3 indicates an improvement in the HRS/LRS ratio of the bilayer device compared to the single-layer device.

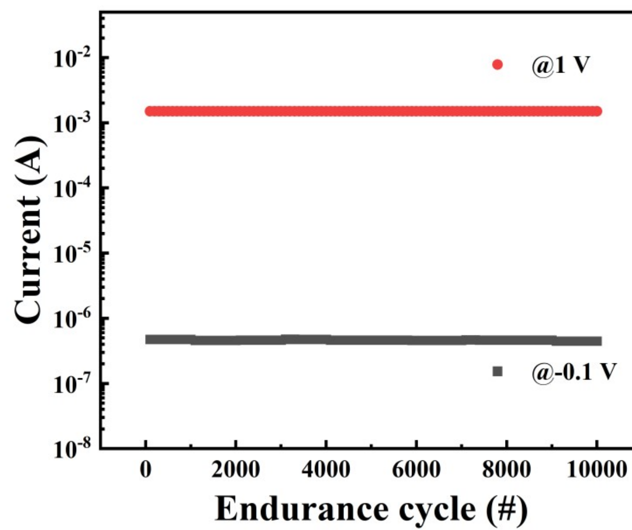

Figure S4 The endurance properties of the TiO_2/ZnO structure.

The endurance properties of the bilayer device, as shown in Figure S4, exhibit significant stability under write voltage at 1 V and read voltage at -0.1 V, showcasing potential applications in neuromorphic computing.

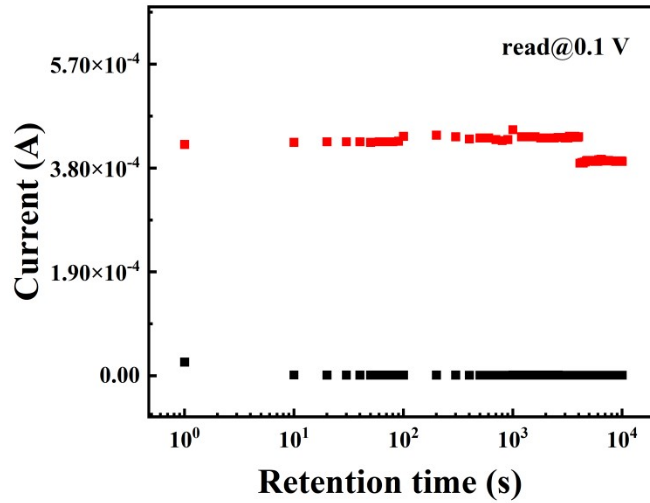

Figure S5 Retention capability of the corresponding HRS and LRS measured in 0.1 V

Figure S5 illustrates the retention capacity measured at 0.1 V, proving that the good retention property for 10^4 s.

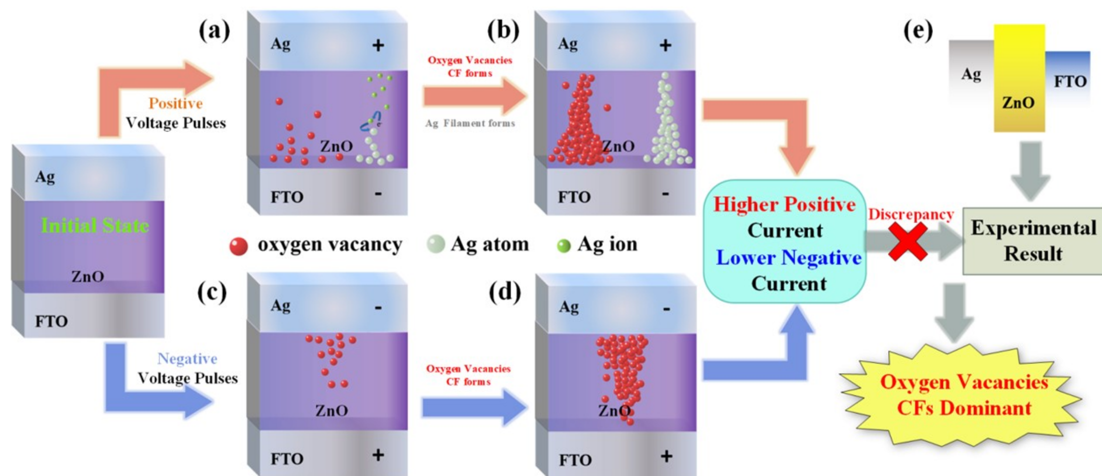

Figure S6 (a) The oxygen vacancies migrate to the bottom electrode, and the Ag^+ are reduced and accumulate on the bottom electrode; (b) Oxygen Vacancies CFs and Ag CFs form; (c) Only oxygen vacancy migration with negative voltage pulses; (d) Oxygen Vacancies CFs form; (e) The schematic diagram of energy band for Ag/ZnO/FTO.

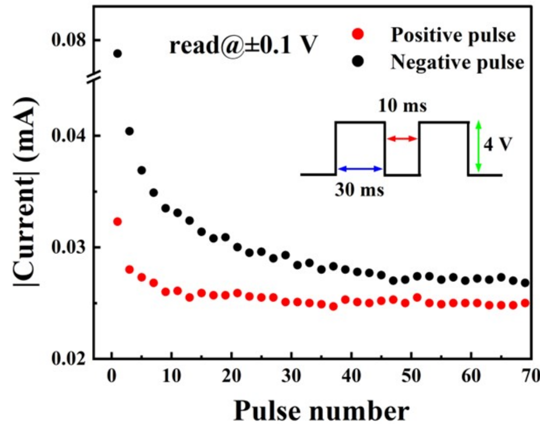

Figure S7 The reading current of Ag/ZnO/FTO memristor when forward pulse and reverse pulse are applied.

We temporarily assume that the active metal CFs and the oxygen vacancy CFs act together on the device resistance switching mechanism. The Ag/ZnO/FTO device is applied a forward pulse voltage in the initial state (Figure S6a). Oxygen vacancies migrate to the bottom electrode, and the active electrode undergoes an oxidation reaction. Ag ions undergo a reduction reaction at the bottom electrode and accumulate. Subsequently, the oxygen vacancy CFs and the Ag CFs are formed together to contribute to the total current (Figure S6b). Otherwise, when the reverse pulse is applied from the initial state, the metal CFs cannot be formed because the bottom electrode is FTO that cannot be oxidized to form an active metal. The oxygen vacancies still migrate under the action of electric field (Figure S6c), and form CFs. Under the reverse pulse, only the oxygen vacancy CFs contribute to the decrease of conductivity. According to the assumed results, the total forward pulse current should be greater than the reverse pulse current. Nevertheless, based on the experimental results depicted in Fig. S7, the reverse pulse current is observed to be greater than the forward pulse current. This contradicts the initially posited hypothesis, rendering it invalid.

Moreover, the VCM, rooted in the migration of oxygen vacancies, is predisposed to engender a persistent resistive switching phenomenon akin to an analog memristor. In contrast, the electrochemical metallization memory (ECM) mechanism, contingent upon the redox processes of active metal electrodes, is more prone to evoke a transient resistive switching behavior, manifested as a digital memristor. In the ZnO-based memristor that we fabricated, the REST process conspicuously manifests as a analog memristor characterized by a gradual alteration in resistance. This phenomenon can be attributed to the incremental disruption of CFs occurring during the migration of oxygen vacancies.

Ultimately, the COMSOL-simulated I-V curve of the oxygen vacancy migration-based memristor, as illustrated in Figure S7, closely aligns with the corresponding experimental findings (Figure 1b). This alignment underscores the significant influence of the VCM in governing the resistance state conversion mechanism within the ZnO-based memristor.

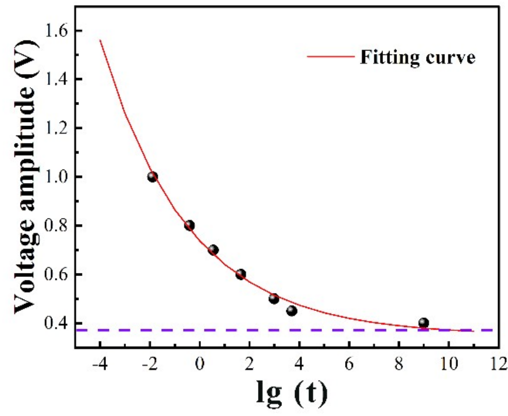

Fig. S8 The relationship between the breaking time of CFs and the change of voltage amplitude.

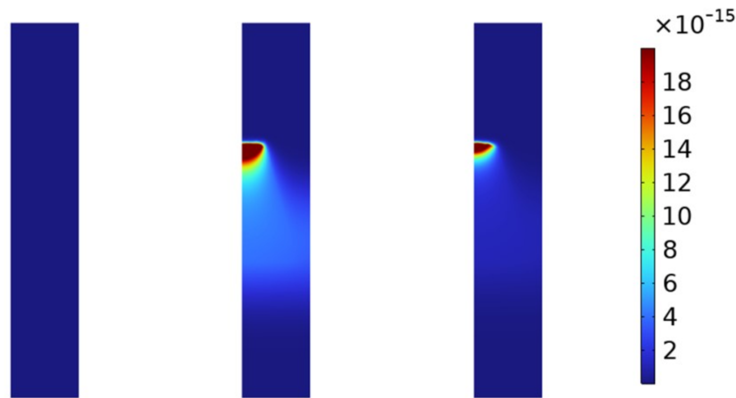

Figure S9 Distribution of oxygen vacancy diffusion coefficient in different time.

The heightened Joule heat facilitated the diffusion of oxygen vacancies in the area where CFs initiated its rupture, accelerating the breakage of the CFs, as demonstrated in Figure S9.

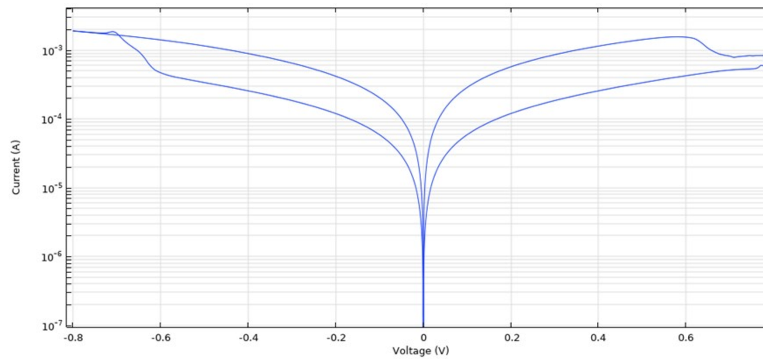

Figure S10 Simulation model I-V scan diagram.

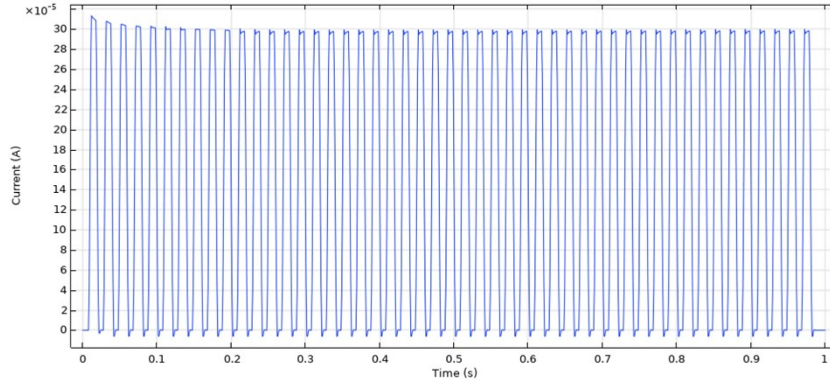

Figure S11 The current response of Ag/ZnO/FTO memristor under 1V@50Hz pulse excitation is simulated by COMSOL.

The electro-thermal coupled memristor model, rooted in the oxygen vacancy diffusion, exhibits I-V curves (Figure S10) and impulse responses (Figure S11) that closely resemble the actual experimental findings.

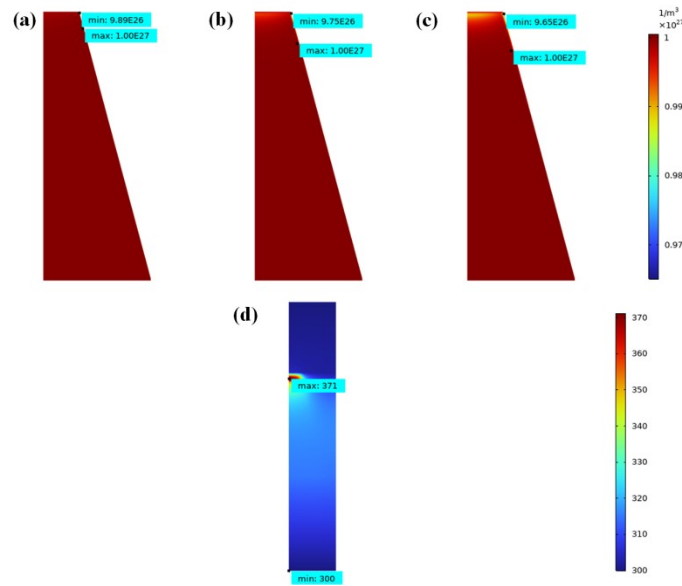

Figure S12 (a-c) The oxygen vacancy concentration changes when the bias voltage of 1V is applied at 2.01s, 6.4s and 20s. (d) Temperature fraction at 20 s.

After applying a 1 V bias in Figure S12, similar to a single-layer ZnO device for 20 seconds, there is no significant change in the concentration of oxygen vacancies within the ZnO layer.